Water Air Soil Pollut (2024) 235:79
https://doi.org/10.1007/s11270-023-06803-w

Construction of OTAB/Bt/TiO_2 Composite Photocatalysts to Improve the Adsorption and Photocatalytic Performance for SCN^- Removal

Tingting Wang · Lucheng Zhang · Mingqing Zhang · Fang Yang · Shilong Wu

Received: 25 August 2023 / Accepted: 5 December 2023 / Published online: 12 January 2024

Abstract The widespread use of cyanidation in gold beneficiation leads to a large amount of SCN^- in the gold extract tail solution, which poses a threat to the environment and human health. The present study successfully synthesized octadecyltrimethylammonium bromide/bentonite/titanium dioxide (OTAB/Bt/TiO_2) photocatalysts through a sol–gel hydrothermal approach. Evaluation of the BET specific surface area, X-ray diffraction (XRD) analysis, UV–vis diffuse reflectance spectroscopy, and zeta potential experiments unveiled the beneficial impact of incorporating OTAB. This inclusion led to an enlargement of the pore size and layer spacing of Bt, broadening the range of photoresponses. Additionally, it effectively neutralized the negative charge residing on the surface of Bt. Consequently, these enhancements contributed to the improved performance of the photocatalytic material in terms of adsorption and catalytic degradation of SCN^-. The degradation rate of SCN^- reached 98.78% under the reaction conditions of initial SCN^- concentration of 50 mg/L, OTAB/Bt/TiO_2 dosage of 0.8 g/L, pH = 8, and reaction time of 300 min. The degradation of the SCN^- composite through the OTAB/Bt/TiO_2 photocatalytic process followed a zero-order kinetic model with a calculated rate constant (k value) of 0.1148 min^{-1}. Notably, this rate constant was 1.9 times greater than the degradation rate observed in the pure TiO_2 system. The free radical quenching test showed that h^+, •OH and $•O^{2-}$ were the main oxidizing substances for photocatalytic degradation. The identification of intermediates proved that the complete mineralization of SCN^- could be achieved by OTAB/Bt/TiO_2 adsorption and photocatalytic degradation without generating the highly toxic intermediate CN^-. Overall, this study provides guidance for the development of more photocatalysts with strong adsorption properties and more effective removal of SCN^- from gold extraction tailings.

Keywords OTAB/Bt/TiO_2 · Adsorption · Photocatalytic · SCN^- · Wastewater treatment

1 Introduction

As cyanide is easy to form different forms of complexes with metallic elements, it is often used as an inhibitor in the flotation process and as a leaching agent for the extraction of gold and silver in the gold beneficiation process (Li, 2018; Tai et al., 2007). During the cyanide leaching process, the metal sulfides react with the cyanate (CN^-) to produce a large amount of thiocyanate (SCN^-) into the gold extract tail solution (Eqs. 1–4) (Wu et al., 2011). Unlike CN^-, the cyanide-breaking process

T. Wang · L. Zhang · M. Zhang (✉) · F. Yang · S. Wu
School of Environment and Spatial Informatics, China University of Mining & Technology, Xuzhou 221116, China
e-mail: zmqcumt@163.com.cn

commonly used for gold extract tail solution treatment is not effective in degrading the more stable SCN^- (Yuan et al., 2021). Chlorination is a common disinfection process for cyanide-containing wastewater. During this treatment process, SCN^-, which cannot be effectively degraded, tends to react chemically with chlorine, as shown in Eq. (5), to produce the highly toxic substance cyanogen chloride, resulting in elevated effluent toxicity and a potential hazard to the health of the operator and the surrounding ecological environment (Pan et al., 2009). Therefore, there is an urgent need for a safe and efficient method to degrade SCN^-.

$$S + CN^- = SCN^- \quad (1)$$

$$2S^{2-} + 2CN^- + O_2 + 2H_2O = 2SCN^{2-} + 4OH^- \quad (2)$$

$$2S + 2OH^- + O_2 = {S_2O_3}^{2-} + H_2O \quad (3)$$

$${S_2O_3}^{2-} + CN^- = {S_2O_3}^{2-} + SCN^- \quad (4)$$

$$SCN^- + 8Cl_2 + 9H_2O = {NO}^{3-} + {SO_4}^{2-} + CO_2 + Cl^- + 18H^+ \quad (5)$$

Several methods have been used to remove SCN^- from wastewater, including biodegradation (Bezsudnova et al., 2007; Combarros et al., 2015; Karavaiko et al., 2000), physical adsorption (Wu et al., 2011), persulfate (Budaev et al., 2015), and photocatalytic (Vohra, 2011) degradation. Adsorption photocatalysis provides a new method for environmental treatment and energy conversion by synergistically degrading organic and inorganic pollutants through photocatalytic redox reactions and adsorption. The technology is currently achieving encouraging results in areas such as lignin removal (Gao et al., 2019), formaldehyde purification (Gu et al., 2019), and waste leachate treatment (Azadi et al., 2020). In addition, the renewable nature of the photocatalyst and adsorbent demonstrates the environmental friendliness and high economic effect of this technology.

Bentonite, an adsorbent material renowned for its porous nature, features montmorillonite as its principal constituent. Embellished with a unique crystal structure consisting of an aluminum-oxygen octahedron layer and twin silica-oxygen tetrahedron layers, its prominence arises from its expansive surface area, exceptional adsorptive capabilities, and potent ion exchange capacity (Bhattacharyya & Sen Gupta, 2008). Consequently, it has been extensively employed in combating environmental contamination, notably heavy metal wastewater (Aminy et al., 2022), dye wastewater (Huang et al., 2017), and electroplating wastewater (Amaya et al., 2020). Esteemed for its cost-effectiveness and ready availability vis-à-vis alternative solids like activated carbon and zeolite, it also marvelously mitigates environmental concerns associated with post-treatment recycling (El-Korashy et al., 2016; Maxim et al., 2016). The uneven substitution of cations within natural bentonite gives rise to anionic interlayers that lack the necessary capacity for the adsorptive elimination of anionic contaminants and hydrophobic substances (Anirudhan & Ramachandran, 2015). Various methods have been introduced to activate natural bentonite, encompassing high-temperature modification (Selim et al., 2020), acid modification (Kaleta et al., 2013), organic modification (Haciyakupoglu & Orucoglu, 2013), and inorganic modification (Tomic et al., 2015). The organic modification of bentonite enables the degradation of a broad spectrum of water pollutants, encompassing the extraction of xylene from industrial wastewater (Ma et al., 2023), the elimination of naphthalene (Kaya et al., 2013), and the adsorption of tetracycline (Alkizwini & Alquzweeni, 2021). Utilizing quaternary ammonium surfactants serves as one of the prevailing techniques for organic modification (He et al., 2023; Olafadehan et al., 2022). By forming feeble hydrogen bonds between the methyl hydrogen atoms on the polar head group of quaternary ammonium surfactants and the surface molecules of bentonite, the anions within the interlayers are effectively neutralized. Octadecy trimethyl ammonium bromide (OTAB) finds widespread utility in the modification of layered clays, owing to its elongated alkyl chain. With the ability to effectively integrate within the interlayers of layered clays or adsorb onto their surfaces, OTAB achieves the formation of a durable structure while altering the hydrophobic milieu between the layers. This transformative action results in a notable expansion of the interlayer spacing, consequently exhibiting exceptional proficiency in the adsorption of various pollutants (Huang et al., 2006; Soegijono, 2017).

Adsorption photocatalysis represents an advanced, highly efficient, enduring, stable, and environmentally sound technology. Through the amalgamation of photocatalytic redox and adsorption, the decomposition of both organic and inorganic pollutants can be accomplished, generating harmless, nontoxic molecules (Lin et al., 2012; Zhuang et al., 2020). In recent years, numerous researchers have undertaken studies on bentonite-based TiO_2 complexes to heighten photocatalytic activity, such as TiO_2-bentonite for the degradation of Rhodamine B (Li Jing-Yi et al., 2007), TiO_2/chitosan/bentonite composite for the adsorption and photocatalytic degradation of methylene blue (Li et al., 2022), and TiO_2/bentonite for the removal of arsenic (Saleh et al., 2021).

In this scholarly endeavor, we embarked on an in-depth exploration and validation of the adsorption and degradation of SCN^- in aqueous milieus, facilitated by the use of OTAB/Bt/TiO_2 composites under the stimulus of UV light irradiation. The investigation was guided by three primary objectives: (1) The utilization of X-ray diffraction (XRD), scanning electron microscopy (SEM), BET-specific surface area measurements, Fourier infrared spectroscopy (FT-IR), and ultraviolet–visible near-infrared spectrophotometry (UV–Vis) to characterize the synthesized OTAB/Bt/TiO_2 composites meticulously; (2) The scrutiny of the influence exerted by the OTAB/Bt/TiO_2 composites' dosage, pH, and initial SCN^- concentration on the efficacious degradation of SCN^- from water; (3) The elucidation of the pathways and mechanisms of SCN^- photocatalytic degradation through the modulation of zeta potential, radical quenching tests, and the identification of intermediate products.

2 Materials and Methods

2.1 Regents

Titanium dioxide (anatase, > 99.5%) and potassium ferricyanide (≥ 99.5%) were obtained from Tianjin Chemical Reagent No. 3 Factory. Sodium bentonite (> 90%) was purchased from Shandong Yusuo Chemical Technology Co. Sodium hydroxide (97%), tetrabutyl titanate (98%), glacial acetic acid (99.5%), ethanol (99.7%), and disodium EDTA (> 99%) were purchased from Shanghai Macklin Biochemical Co., Ltd. Sodium hydroxide (97%), octadecyltrimethylammonium bromide (OTAB, 99%), anhydrous ethanol (99.7%), isopropanol (99.5%), silver nitrate (0.1 mol/L), and p-benzoquinone (99.5%) were purchased from Shanghai Aladdin Biochemical Technology Co., ltd, China. Hydrochloric acid (HCl) was purchased from Sinopharm Chemical Reagent Co., ltd, China. Milli-Q water (> 18 MΩ·cm) was used to prepare different solutions of required concentrations.

2.2 Preparation of Photocatalysts

2.2.1 Synthesis of OTAB/Bt Materials

A specified quantity of OTAB is dissolved in water and combined with 5 g of sodium bentonite, undergoing stirring for a duration of 3 h. After the reaction is completed, the resulting slurry is diligently washed with ultrapure water until the absence of boron ions is confirmed, prior to filtration through a water recirculation vacuum pump. The filtrate is subsequently dried at 90 °C for a period of 12 h. Finally, the sample is finely ground to pass through a 200 mesh sieve, yielding the OTAB/Bt powder.

2.2.2 Synthesis of OTAB/Bt/TiO_2 Composite Photocatalysts

The synthesis of the photocatalyst OTAB/Bt/TiO_2 was performed using the sol–gel hydrothermal method outlined as follows: A: 10 mL of tetra butyl titanate and 2 mL of glacial acetic acid were dissolved in a solution of 20-mL anhydrous ethanol. B: A solution of 13.23-mol/L anhydrous ethanol was prepared. The dispersion of 2.5 g of OTAB/Bt powder (with a cation exchange capacity of 0.4) was dissolved into liquid A. Liquid B was then gradually added drop by drop to liquid A. The resulting mixture was subjected to magnetic stirring for 24 h at room temperature, resulting in the formation of a yellow gel. Subsequently, the gel was allowed to age for 8 h before being transferred into a reactor and subjected to hydrothermal reaction at 120 °C for 12 h. Afterward, it was allowed to cool down to 25 °C and washed three times with ultrapure water. The sample was filtered by a vacuum water circulation pump, dried overnight at 90 °C, ground, and passed through a 200-mesh sieve to obtain OTAB/Bt/TiO_2 photocatalyst. The preparation process of OTAB/Bt/TiO_2 photocatalysts is shown in Fig. 1.

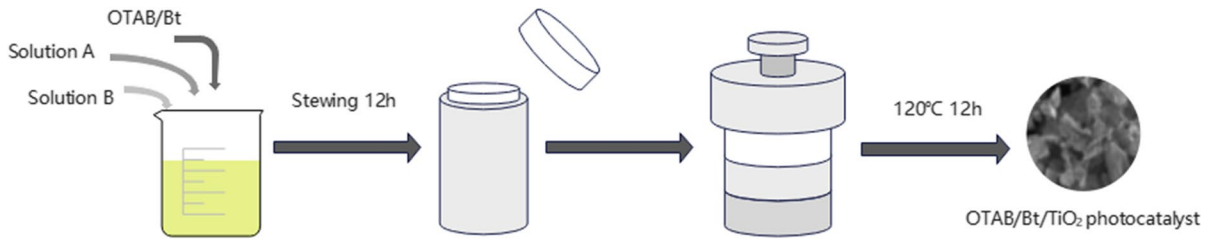

Fig. 1 The preparation diagram of OTAB/Bt/TiO_2 photocatalyst

2.3 Characterization

X-ray diffraction (XRD, D8 ADVANCE, Germany) was used to determine the crystallinity and phase structure of the samples using a copper target (40 kV, 30 mA) with a scanning range of 3–80° and a scanning rate of 8°•min^{-1}. The micromorphology of the samples was observed using a scanning electron microscope (SEM, Quanta 250, USA). The specific surface area of bentonite before and after modification was obtained by analyzing the nitrogen adsorption–desorption isotherm (BET, ASAP2460, Shanghai, China) at 77.3 K and an equilibrium interval of 10 s. The pore size of the bentonite was calculated as the amount of N_2 adsorbed ($p/p_0 = 0.99$). The infrared spectra of bentonite and modified bentonite were obtained using a Fourier infrared spectrometer (FT-IR, VERTEX 80v, Bruker, Germany). UV–Vis diffuse reflectance spectra were acquired on a UV–Vis near infrared spectrophotometer (UV–Vis, UV-2600-ISR-Plus, Japan) to obtain the light absorption properties of the different catalysts, with a scanning wavelength range of 200–800 nm.

2.4 Experimental Procedure

The evaluation of the photocatalytic activity of OTAB/Bt/TiO_2 was conducted by measuring the degradation of SCN^- in an aqueous solution. For this purpose, a 175W UV high-pressure mercury lamp (manufactured by Shanghai Mingyao Glass Hardware Tools) was utilized as the light source. The experimental setup is illustrated in Fig. 2. To initiate the experiment, 0.8 g of OTAB/Bt/TiO_2 was dispersed in SCN^- simulated wastewater (150 mL, with an initial SCN^- concentration of 50 mg/L) and positioned directly beneath the UV lamp. Prior to exposure to light, the suspension was subjected to magnetic stirring for 30 min, allowing for the establishment of an adsorption–desorption equilibrium of SCN^- on the surface of OTAB/Bt. This step, referred to as the dark reaction. Following the equilibration period, the UV lamp was activated and the suspension was continuously stirred for 5 h. During the

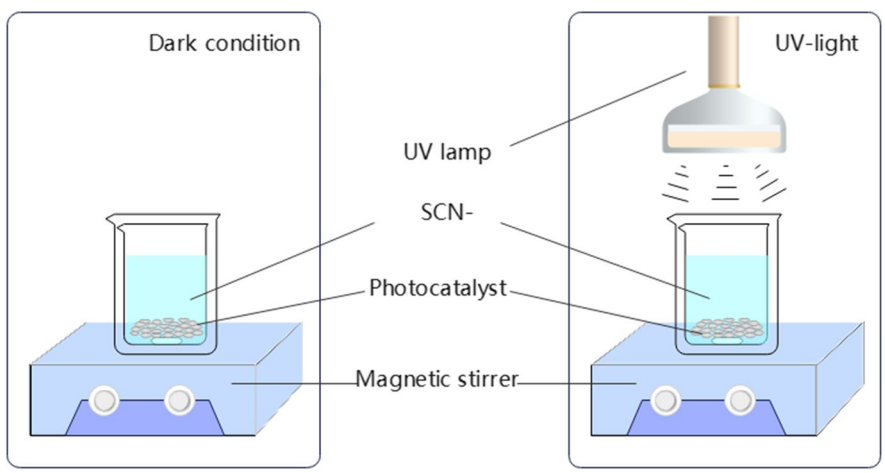

Fig. 2 Schematic diagram of photocatalytic degradation test device

degradation process, 2-mL samples were withdrawn from the photocatalytic system at hourly intervals using a pipette gun, in order to perform subsequent analysis.

2.5 Analysis

The absorbance of SCN^- was measured at 452 nm using a visible spectrophotometer (722, China). A standard curve (7 concentration gradients): The baseline of solvent water was established, a set volume of SCN^- solution (2 ml) was injected, and Fe $(NO_3)_3$ solution (7 mL, 50 g/L) was added, shaken well, and the color was developed in a dark environment for 5 min. Absorbance was measured, the concentration was taken as the abscissa, the corrected absorbance was taken as the abscissa, and the standard curve was plotted, as shown in Fig. 3. Sample determination, the sample to be measured was filtered through a 0.45-μm polyethersulfone filter (the color development process was consistent with that of the standard sample), placed in a 10-mm quartz cuvette, and the absorbance of residual SCN^- was corrected using ultrapure water as the blank reference. The concentration of residual SCN^- in the sample was determined from the standard curve equation and the absorbance (corrected). The removal efficiency was calculated as follows (Eq. 6):

$$\gamma_1 = \left(C_0 - C_t\right)/C_0 * 100\% \quad (6)$$

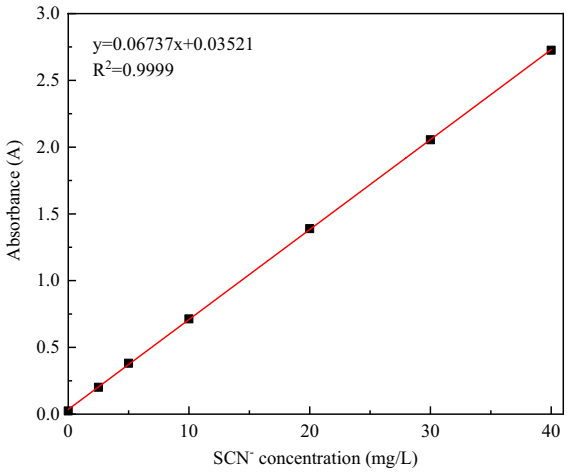

Fig. 3 Standard curve of SCN^- concentration

where, γ_1 is the SCN^- removal rate (%); C_0 is the initial SCN^- concentration (mg/L); C_t is the SCN^- concentration (mg/L) at reaction time t.

3 Result and Discussion

3.1 Characterization

Figure 4 presents SEM images of Bt, OTAB/Bt, and OTAB/Bt/TiO_2. In Fig. 4a, b, c, it can be observed that Bt exhibits a smooth and layered structure, while the surface of OTAB/Bt appears rough. Notably, OTAB/Bt/TiO_2 displays a granular structure with particles of varying sizes and uneven distribution, along with the presence of a pore structure (Mishra et al., 2017). It can be seen that the introduction of OTAB/TiO_2 disrupts the crystalline surface order of Bt (001), forming more crystalline sequences, and no significant agglomeration of TiO_2 occurs. Additionally, the structure of OTAB/Bt/TiO_2 prepared by sol–gel method facilitates the convenient channeling of electrons during the reaction, thereby enhancing the rate of photogenerated electron–hole separation (Gao et al., 2020).

Additionally, unlike the energy-dispersive X-ray spectroscopy (EDS) pattern of Bt, the EDS pattern of OTAB/Bt/TiO_2 clearly displays characteristic peaks of Ti alongside the characteristic ions (Si, Al, Mg, Ca, C) of OTAB/Bt. This further confirms the successful attachment of TiO_2 nanoparticles onto the surface of OTAB/Bt, as depicted in Fig. 4d, e, f. Also, the distribution of titanium is more homogeneous (Fig. 4g). Fascinatingly, our analysis of the OTAB/Bt/TiO_2 composite revealed the absence of Na^+ ions and a reduction in the quantity of K^+ ions. This phenomenon can potentially be attributed to the substitution of the inorganic cation Na^+ within the interlayer of Bt by the positively charged groups present in OTAB. Remarkably, similar occurrences have been documented in other literature sources, further supporting this observation (García-García et al., 2023).

The determination of specific surface area and pore size distribution of the materials was conducted using the multi-point BET method, and the results are summarized in Table 1. The specific surface area of OTAB/Bt exhibited a reduction to 1.2646 m^2/g, and the total pore volume experienced a change to 0.0065 cm^2/g when compared to Bt alone. The incorporation

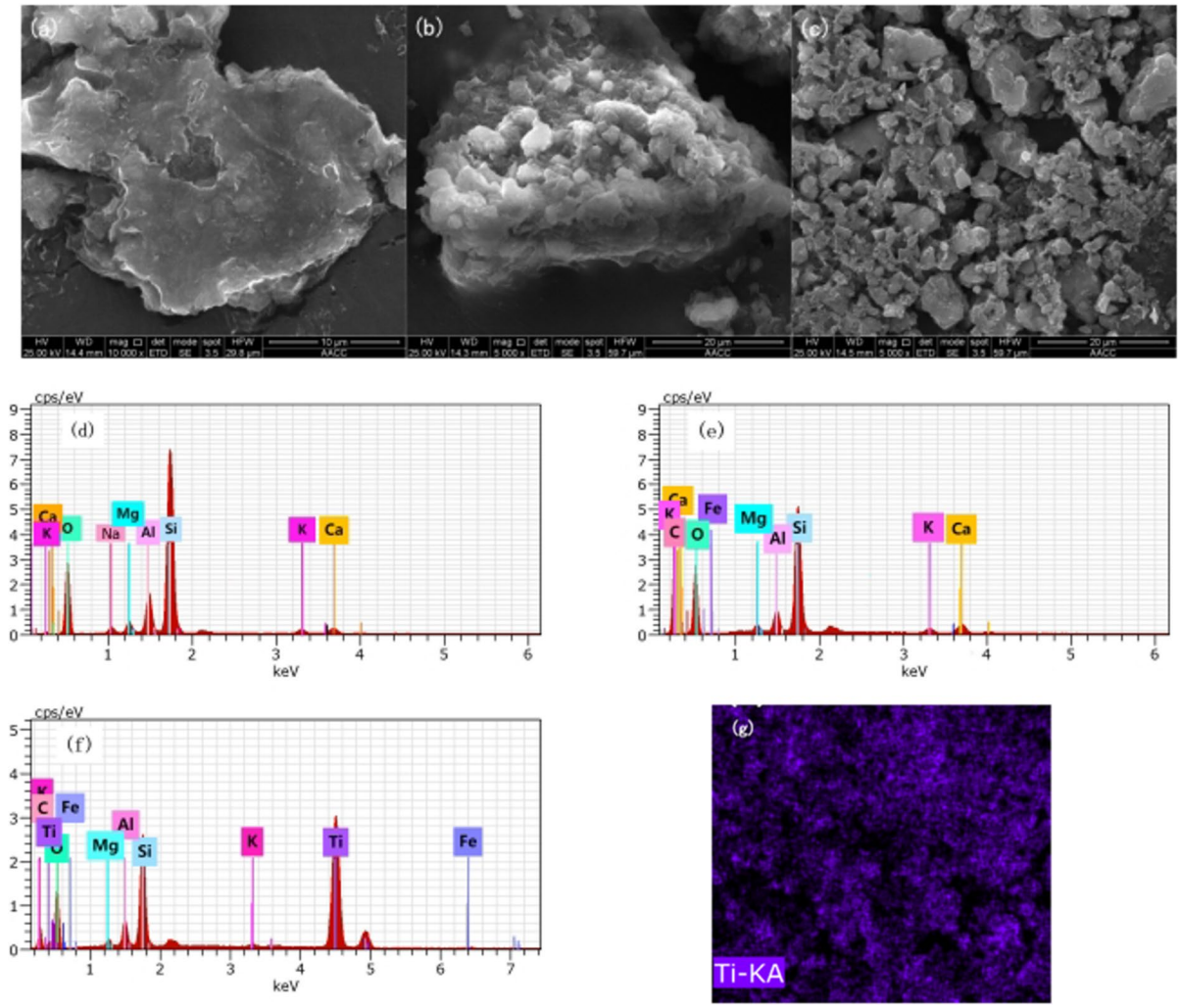

Fig. 4 SEM images and EDS-mapping of samples: **a**–**d** Bt; **b**–**e** OTAB/Bt; **c**–**f** OTAB/Bt/TiO_2; **g** Ti elements

Table 1 The analysis of Bt and organic bentonite

Sample	Specific surface area (m^2/g)	Pore diameter (nm)	Pore volume (cm^2/g)	Zeta potential (mV)
Bt	50.8947	6.7367	0.0586	−30
OTAB/Bt	1.2646	14.6156	0.0065	17

of OTAB brought about the aggregation of crystals on the Bt surface, resulting in the formation of clustered structures and a subsequent modification of the original layered arrangement. This alteration in structure contributed to the observed decrease in specific surface area and pore volume, findings that align with the scanning electron microscopy (SEM) results. However, it is noteworthy that the presence of OTAB also led to a twofold increase in the average pore size, enhancing the overall capacity for adsorption by creating a larger adsorption space. Furthermore, in the adsorption of SCN^-, electrostatic interactions emerged as a crucial factor. The zeta potential results presented in Table 1 indicate that the positively charged groups of OTAB effectively neutralize all the negative sites on the surface of Bt, rendering the OTAB/Bt composite positively charged. This positive charge facilitates the efficient adsorption of negatively charged SCN^- ions.

Figure 5a illustrates the X-ray diffraction (XRD) patterns of Bt, OTAB/Bt, and OTAB/Bt/TiO_2. The distinctive diffraction peaks (2θ) for the pristine Bt and OTAB/Bt were observed at 7.038° and 4.229°, respectively. Notably, the layer spacing of OTAB/Bt (2.088) was found to be larger than that of the pristine Bt (1.255), as calculated using Bragg's equation ($n\lambda = 2d\sin\theta$). This observation indicates that the introduction of OTAB can enhance the layer spacing of Bt, thereby improving the adsorption capabilities of the photocatalytic material for SCN^- and ultimately enhancing its photocatalytic activity. Moreover, in the XRD pattern of OTAB/Bt/TiO_2, distinct diffraction peaks were observed at 25.4°, 37.9°, and 55.2°, corresponding to the crystal planes (101), (004), and (211) of anatase-type TiO_2. This signifies the successful synthesis of anatase-type TiO_2 in the OTAB/Bt matrix (Wang et al., 2012). No other diffraction peaks (rutile-type TiO_2) were detected in OTAB/Bt/TiO_2, affirming the good crystallinity and high purity of anatase TiO_2 in OTAB/Bt/TiO_2 (Du et al., 2019).

Figure 5b displays the Fourier-transform infrared (FT-IR) spectra of various photocatalytic materials. The absorption peaks observed at 2918 cm^{-1} and 2850 cm^{-1} correspond to the -CH_2 antisymmetric stretching vibration and the -CH_3 symmetric stretching vibration peaks of OTAB, respectively. The absorption peaks within the wave number range of 1100–1000 cm^{-1} are commonly associated with the stretching vibrations of Si–O-Si and Si–O-Al. As a result, the intensity of the absorption peaks observed in OTAB/Bt and OTAB/Bt/TiO_2 remains relatively stable within this range when compared to Bt.

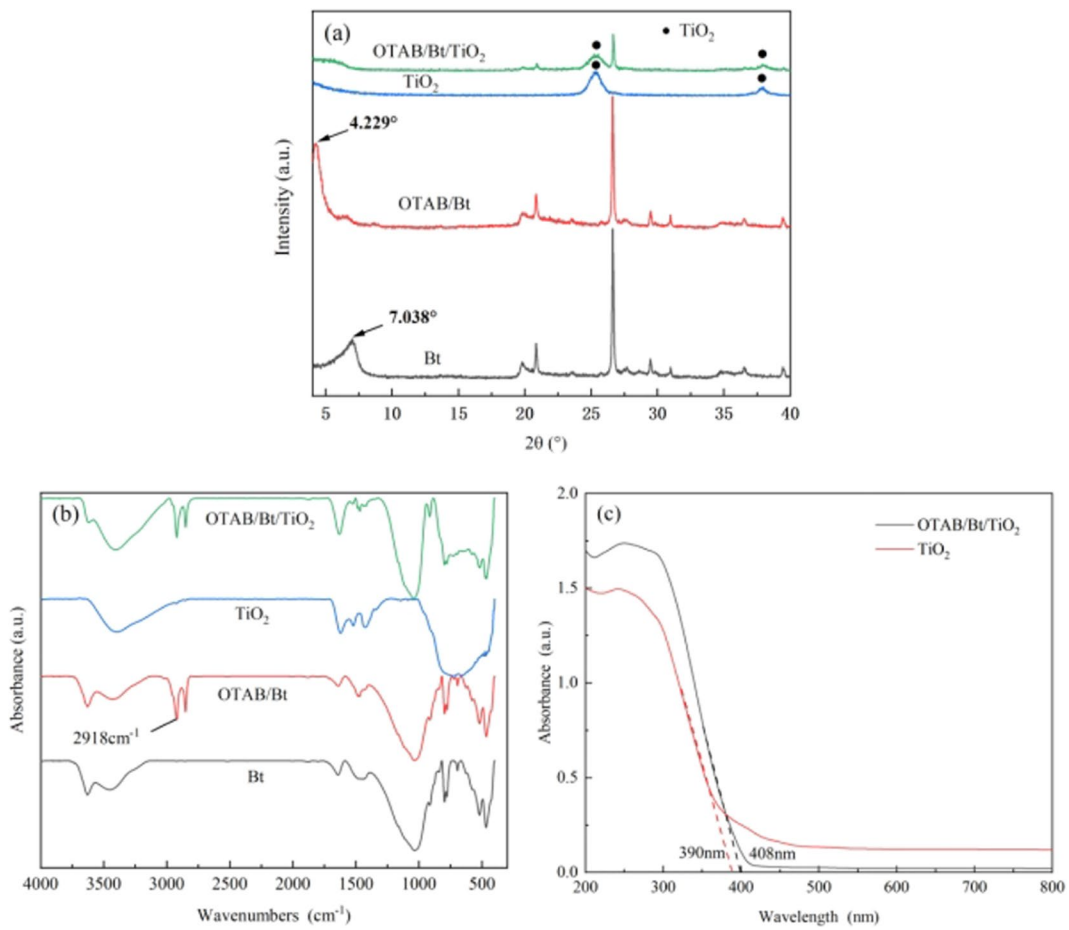

Fig. 5 **a** X-ray diffraction (XRD) patterns; **b** Fourier transform infrared spectroscopy (FTIR) spectra; **c** ultraviolet–visible diffuse reflectance spectra

Vibration peaks within the range of 500–800 cm^{-1} can be attributed to the Ti–O bond. Moreover, in the FT-IR spectra of TiO_2 and OTAB/Bt/TiO_2, distinctive peaks at 1500 cm^{-1} and 3500 cm^{-1} are indicative of the stretching of the -OH bond. These peaks predominantly arise from the attachment of hydroxide ions and hydroxyl groups on TiO_2 to the Bt surface.

In Fig. 5c, the ultraviolet–visible diffuse reflectance spectra are depicted to explore the efficacy of various photocatalytic materials in harnessing visible light. The conventional TiO_2 exhibits an absorption band edge located at 390 nm. However, upon integration with OTAB/Bt, an intriguing phenomenon occurs as the absorption band edge undergoes a redshift, with the peak now observed at 408 nm. Consequently, this redshift extends the range of photoresponse (Kuo et al., 2021). Remarkably, the utilization of OTAB/Bt in conjunction with TiO_2 results in an exceptional visible-light response. This attribute amplifies the efficacy of its photocatalytic activity, thereby facilitating the subsequent degradation of SCN^- (Jiang et al., 2022).

3.2 Analysis of Photocatalytic Performance of OTAB/Bt/TiO_2

3.2.1 Comparison of the Photocatalytic Properties of $TiO_2$and OTAB/Bt/TiO_2

The catalytic efficacy of the OTAB/Bt/TiO_2 photocatalysts was assessed through the removal of SCN^- from the aqueous phase via photocatalysis after exposure to UV high-pressure mercury lamps, with TiO_2 utilized as a benchmark. The results of the photocatalytic experiments are depicted in Fig. 6a. The outcomes of the dark reaction revealed that OTAB/Bt/TiO_2 exhibited commendable adsorption performance towards SCN^- (20.03%), facilitating the binding of SCN^- to active sites and thereby enhancing the photocatalytic performance. In the absence of a catalyst, Bt removed only 10% of SCN^- after 300 min of photocatalytic reaction. The catalytic degradation effect of OTAB/TiO_2 (27.98%) was inferior to that of pure TiO_2 (52%) due to the limited modulation of TiO_2 by OTAB, and the presence of OTAB impeded the reaction between SCN^- and active radicals. The influence of TiO_2/Bt on SCN^- degradation was marginally superior to that of pure TiO_2, but it exhibited a significant disparity when compared to OTAB/Bt/TiO_2 (59.11% vs. 98.78%). The surface area ratio and adsorption capacity of Bt/TiO_2 were constrained, necessitating the incorporation of OTAB into Bt. The photocatalytic efficiency of the OTAB/Bt/TiO_2 material was improved by uniformly dispersing TiO_2 on Bt, which reduced the long-range diffusion of free radicals in the solution and enhanced light utilization efficiency. The uniform loading of TiO_2 on OTAB/Bt/TiO_2 exposed a higher number of active sites, while the aggregation of pure TiO_2 in water impeded the interaction of active sites with SCN^-. Moreover, the continuous adsorption and oxidation of

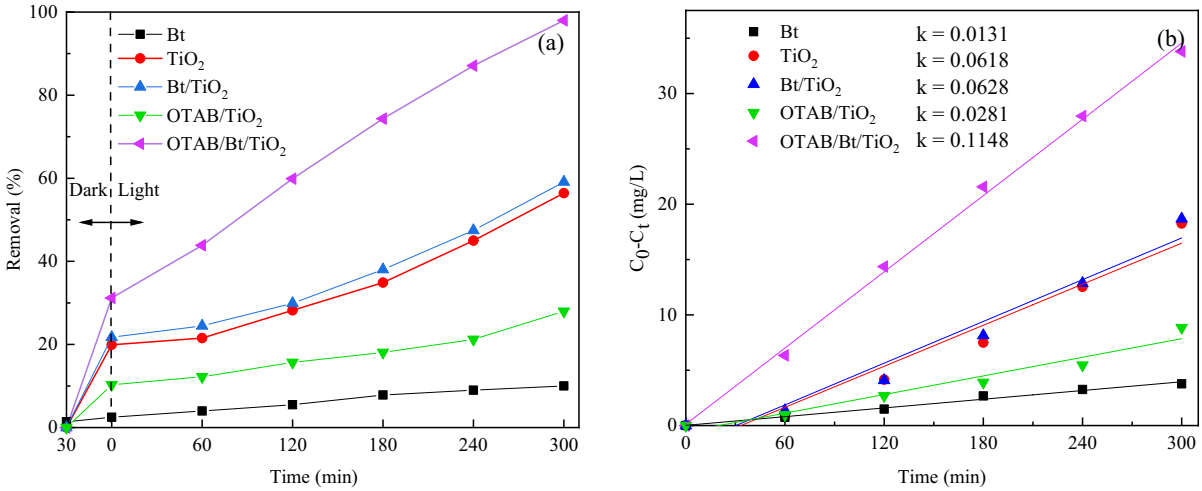

Fig. 6 **a** Removal efficiency and **b** pseudo-zero-order kinetic fitting of SCN^- in various reaction systems tested under UV light irradiation

SCN^- facilitated the migration of substances on the photocatalyst's surface, which inhibited the complexation of photogenerated electrons and holes in TiO_2, ultimately achieving efficient treatment of SCN^-.

To delve deeper into the photocatalytic efficacy of OTAB/Bt/TiO_2, the reaction kinetics were simulated employing a zero-order kinetic equation as depicted below.

$$C_0 - C_t = kt \tag{7}$$

where C_t is the pollutant concentration at time t (mg/L), C_0 is the initial pollutant concentration (mg/L), t is the reaction time, and k is the apparent zero-level kinetic reaction constant.

As represented in Fig. 6b, the OTAB/Bt/TiO_2 photocatalytic degradation of SCN^-composite zero-order kinetics ($R^2 > 0.95$) with a k value of 0.1148 min^{-1} was 1.9 times higher than the degradation rate of the pure TiO_2 system (0.0618 min^{-1}), which further demonstrated the excellent photocatalytic performance of OTAB/Bt/TiO_2.

3.2.2 *Analysis of Factors Affecting Photocatalytic Degradation Efficiency*

Figure 7a illustrates the impact of composite dosage on SCN^- photocatalytic degradation. As the dosage of OTAB/Bt/TiO_2 escalated from 0.2 to 0.8 g/L, the rate of SCN^- degradation exhibited a remarkable surge from 57.41 to 98.78%. This enhanced photocatalytic degradation efficiency can be attributed to the augmented adsorption capacity of the composites and the proliferation of reactive sites. However, when the dosage reached 1.0 g/L, the SCN^- degradation efficiency experienced a decline. This decrement can be ascribed to the excessive dosing, which led to the aggregation of some photocatalyst particles, impeding the interaction and reaction between the pollutants and the active substances. Furthermore, the scattering of ultraviolet light proved unfavorable for the progression of the photocatalytic reaction. Taking into account both economic and effective factors, the optimal dosage of the composite material was determined to be 0.8 g.

The initial pH of the solution exerted an influence on the photocatalytic performance by modulating the generation of active radicals during the OTAB/Bt/TiO_2 photocatalytic process. As depicted in Fig. 7b, the photodegradation efficiency of SCN^- exhibited a decline with an increase in pH within the pH range of 8 to 12 for the investigated system. Notably, at pH 8, the degradation rate of SCN^- reached a remarkable 98.78%, whereas at pH 12, it plummeted to a mere 11.98%. This observation indicates that in highly alkaline solution environments (pH 11 and 12), the •OH radical undergoes a reaction with OH^- in the solution, resulting in the generation of less reactive O^- (Eq. 8), which exerts an inhibitory effect on the photocatalytic degradation of SCN^-.

$$\bullet OH + OH^- = O^- + H_2O\left(pK = 10^{11.9}\right) \tag{8}$$

The initial concentration of SCN^- plays a pivotal role in the photocatalytic degradation of OTAB/Bt/TiO_2. As depicted in Fig. 7c, the elimination of SCN^- escalated from 46.5 to 62.2 mg/L, and the adsorption capacity rose from 8 to 11 mg/g as the SCN^- concentration increased from 50 to 100 mg/L. This phenomenon can be attributed to the fixed number of effective active sites within the OTAB/Bt/TiO_2 (0.8 g). When the initial concentration of SCN^- reached 100 mg/L, the adsorption capacity on the surface of the composite material reached equilibrium. As the SCN^- concentration continued to rise, the pollutant molecules impeded the propagation of light, resulting in a decrease in light transmittance and penetration depth (Chen et al., 2017). Consequently, when the SCN^- concentration increased from 100 to 400 mg/L, the adsorption capacity remained stable, while the removal rate decreased by 4 mg/L.

3.3 OTAB/Bt/TiO_2 Removal of SCN^- Reusability

Taking into consideration the economic and environmental aspects of the actual wastewater treatment process, it is imperative to assess the stability and reusability of catalysts through cyclic degradation tests of OTAB/Bt/TiO_2. Following the photocatalytic degradation test, the OTAB/Bt/TiO_2 present in the solution was recovered via filtration, washed with ultrapure water, and subsequently reused after undergoing drying in an oven at 90 °C for 10 h. This recycled OTAB/Bt/TiO_2 was then employed in the subsequent photocatalytic degradation test. After three cycles of testing, it can be observed that the removal efficiency of SCN^- exhibited no significant changes, decreasing from 98.78 to 95.37% (Fig. 7d). The decline in photocatalytic efficiency can be attributed to two factors:

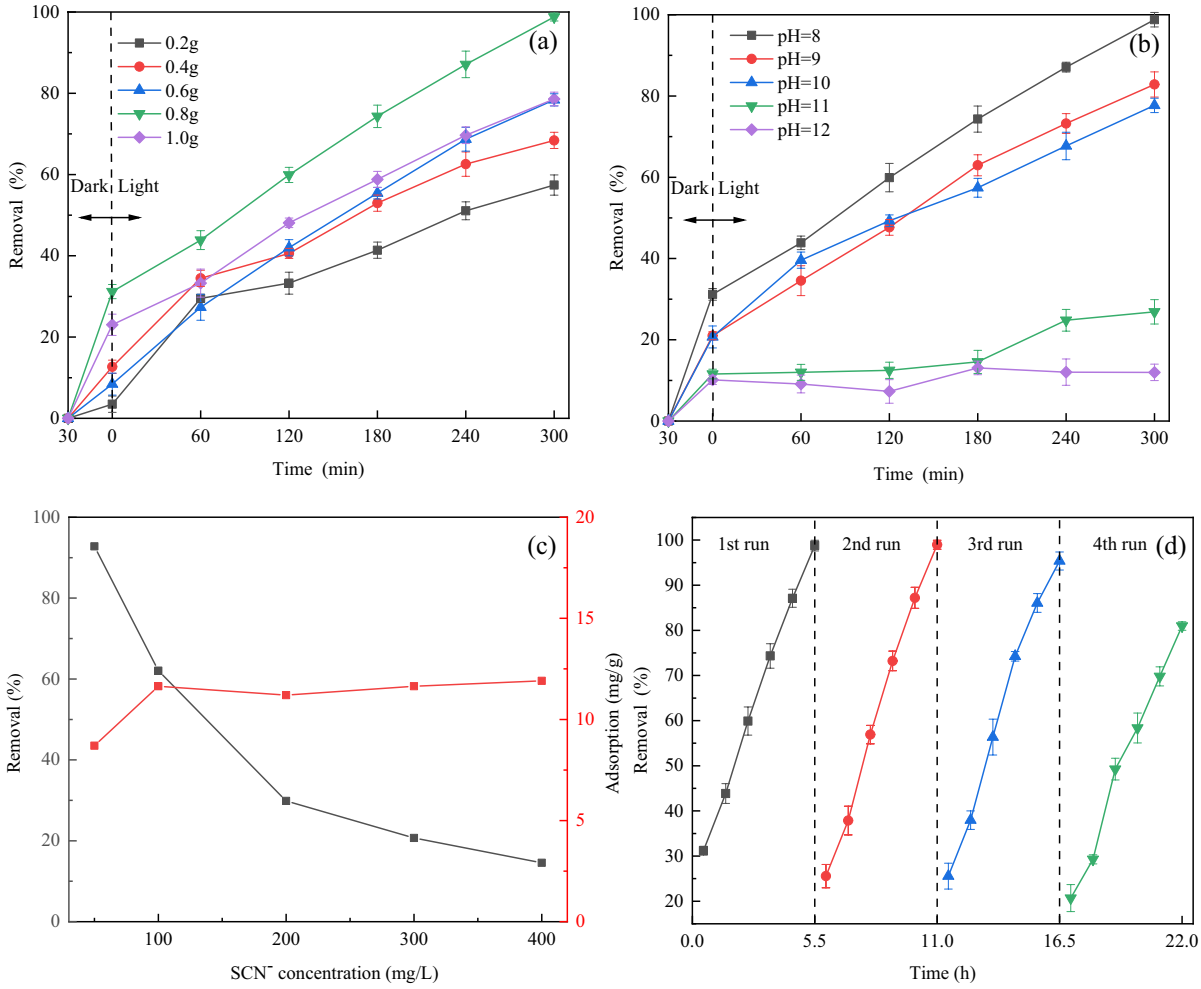

Fig. 7 Photocatalytic degradation efficiency of SCN^- **a** optimization of OTAB/Bt/TiO_2 dosage; **b** effect of pH; **c** effect of initial concentration of SCN^- **d** cycling performance of catalysts (OTAB/Bt/TiO_2 = 0.8 g, pH = 8, $SCN.^-$ = 50 mg/L)

firstly, the loss of catalyst resulting in decreased crystallinity, diminished crystal quality, and reduced stability of TiO_2, thereby suppressing the photocatalytic activity and photoelectric conversion efficiency of the composites; Secondly, certain degradation intermediates that occupy the active sites and pores persistently adhere to the washed and recovered OTAB/Bt/TiO_2, which may lead to a decrease in the photocatalytic ability of the material. Remarkably, even in the fourth cycle test, OTAB/Bt/TiO_2 was still capable of removing 80% of SCN^-. This indicates its high stability and reusability in the photocatalytic process, which makes it competitive among the reported photocatalytic materials (Table 2). Consequently, it holds promising value and prospects for industrial production applications (Pandey, 2017).

3.4 Degradation Mechanisms

3.4.1 Quenching Test

Various radical burst tests were conducted to investigate the role of different reactive groups in the photocatalytic degradation process. To differentiate the oxidation of ·OH, photogenerated electrons (e^-), photogenerated holes (h^+), and $\cdot O_2^-$, 0.5 mmol/L isopropanol (IPA), $AgNO_3$, disodium

Table 2 Comparison of cycling performance of OTAB/Bt/TiO_2 with reported bentonite-based photocatalysts

TiO_2/clay composite	Pollutant (mg/L)	Cycle number	Removal (%)	Ref
OTAB/Bt/TiO_2	Thiocyanide Ion (50)	4	80	This work
TiO_2/Fe_3O_4/benonite	Methylene blue (30)	4	82	(Chen et al., 2015)
Ag/WO_3/Bent	Humic acid (30)	5	75	(Ajel & Al-Nayili, 2022)
A-TiO_2-BiOBr-Bt	Phenol (20)	6	83	(Dlamini et al., 2022)
Fe_2O_3-B-TiO_2	Methyl blue (10)	4	78	(Cao et al., 2017)

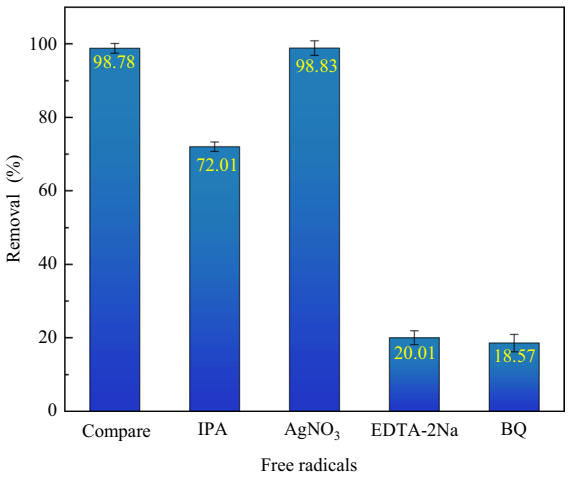

Fig. 8 Effects of different scavengers on the photocatalytic degradation efficiency for SCN^-

ethylenediaminetetraacetic acid (EDTA-2Na), and p-benzoquinone (BQ) were added (Guo et al., 2022). Figure 8 illustrates the results of these tests. In the absence of any bursting agent (control), the degradation efficiency of SCN^- was 98.78%. The addition of $AgNO_3$ had no significant impact on the photocatalytic degradation of SCN^-, indicating that the oxidation of e^- can be ruled out as a contributing factor. However, the presence of IPA hindered the degradation of SCN^-, resulting in a reduction in removal efficiency by 26.77%. This suggests that ·OH groups do contribute to the photocatalytic degradation process, albeit not as the primary oxidizing agents. On the other hand, when EDTA-2Na was introduced into the photocatalytic system, a significant decrease in SCN^- degradation efficiency to 20.01% was observed, highlighting the crucial role of photogenerated holes (h^+) as the main active groups in the photocatalytic degradation of SCN^-. Additionally, the addition of BQ also considerably inhibited the photocatalytic activity, leading to a reduction in degradation efficiency to 18.57%. This finding suggests that $\cdot O_2^-$ is another contributing factor to the removal of SCN^-.

3.4.2 Analysis of the Main Transformation Products and Degradation Mechanisms of SCN^-

Based on the change rule of zeta potential on the surface of the photocatalytic materials, the results of free radical quenching test, and the changes of intermediate product concentration during the photocatalytic degradation process (Fig. 9), the possible pathways of SCN^- degradation by photocatalysis of OTAB/Bt/TiO_2 were inferred (Fig. 10).

Firstly, during the adsorption stage and the early stages of photocatalytic degradation, there exists a strong electrostatic interaction between SCN^- (high electronegativity) and OTAB/Bt (positively charged). This leads to the selective adsorption of SCN^- on the surface of OTAB/Bt/TiO_2, resulting in a decrease in the zeta potential on the photocatalytic material's surface. Secondly, the free radical burst test revealed the involvement of both $\cdot O_2^-$ and ·OH in SCN^- removal, with h^+ and $\cdot O_2^-$ acting as the primary active species. When the photocatalyst is irradiated by the UV light source, electrons in the valence band of TiO_2 undergo a transition to the conduction band, generating e^- and h^+ in OTAB/Bt/TiO_2. The h^+ species possess strong oxidative properties, directly oxidizing adsorbed H_2O and O_2 on the surface into hydroxyl radicals (·OH), superoxide radicals ($\cdot O_2^-$), and other potent oxidizing species (Hirakawa & Nosaka, 2002). Ion chromatography was employed to analyze the SCN^-, SO_4^{2-}, NO^{3-}, NO^{2-}, CN^-, and NH_4^+ present in the photocatalytic degradation samples of OTAB/Bt/TiO_2. Under the influence of ·OH and $\cdot O_2^-$, SCN^- gradually underwent degradation. As depicted in the figure, the concentration of SO_4^{2-} increased from 0 to 30 mg/L (after 300 min of light exposure), and elemental

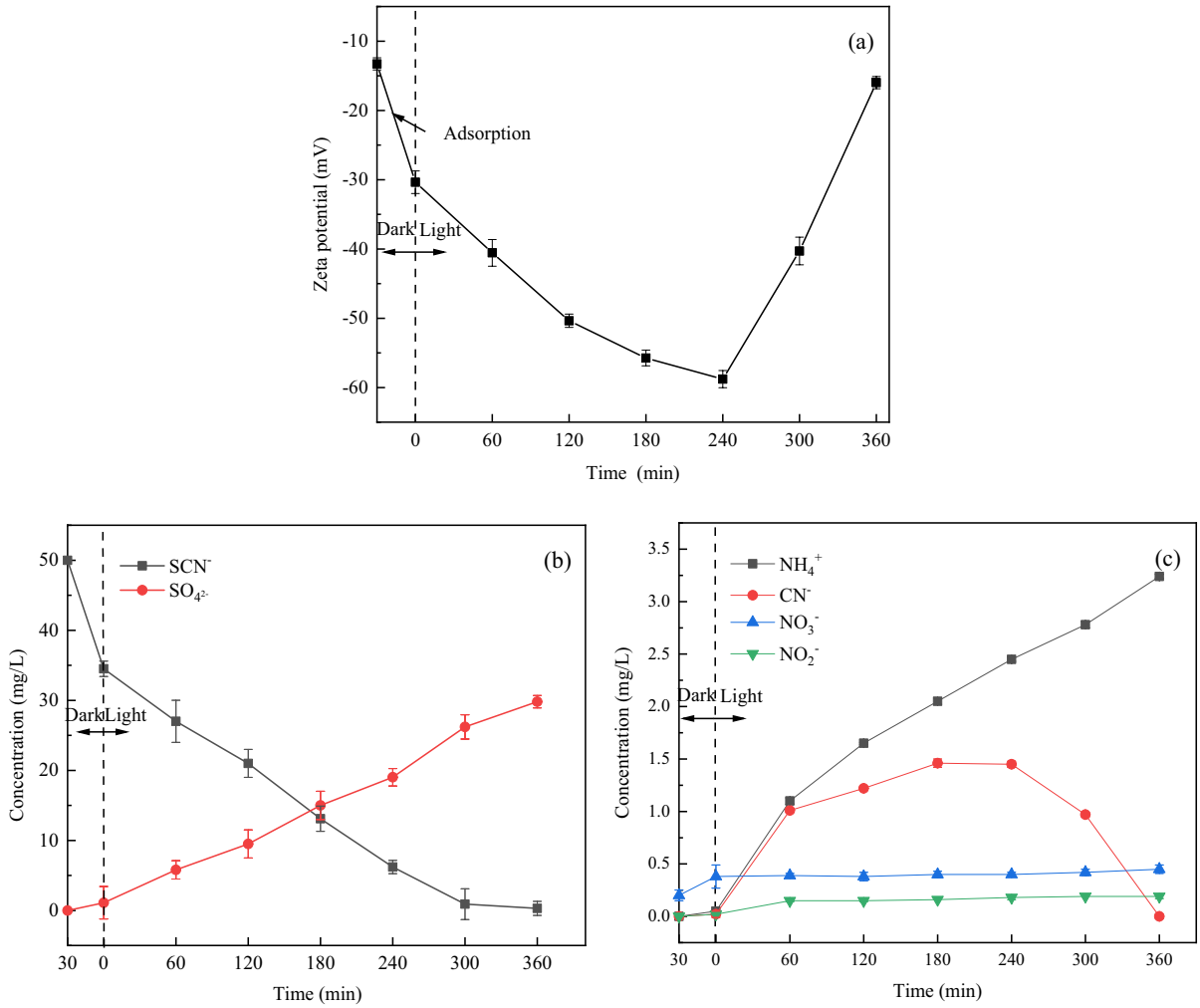

Fig. 9 **a** Zeta potential; **b–c** intermediate product during the photocatalytic degradation process

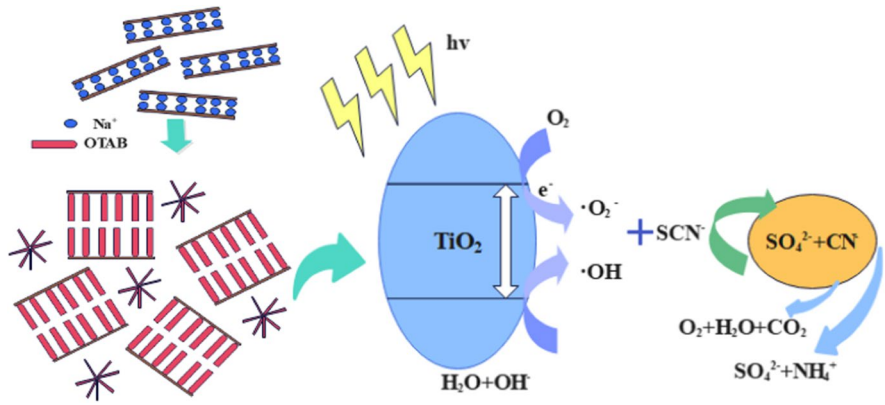

Fig. 10 Possible mechanism diagram of degradation toward SCN^- over OTAB/Bt/TiO_2 photocatalyst

sulfur was ultimately converted to SO_4^{2-}, with a portion escaping as SO_2 gas. Concurrently, as the photocatalytic reaction progressed, the concentration of CN^- gradually rose, eventually reaching a production rate that matched the oxidation rate. CN^- was continuously oxidized to NH^{4+}, CO_2, and H_2O, accompanied by a small amount of NO^{3-} and NO^{2-} production, until CN^- was completely converted. NH^{4+} then became the primary form of nitrogen in the SCN^- samples.

4 Conclusion

In this research endeavor, an innovative adsorption photocatalytic material, namely OTAB/Bt/TiO_2, was successfully synthesized through a simple hydrothermal method. Optimal reaction conditions facilitated the material's impressive ability to adsorb and photodegrade up to 98.78% of SCN^- ions, surpassing the performance of the original sample. This remarkable photodegradation efficacy can be attributed to the following pivotal factors: (1) OTAB/Bt/TiO_2 exhibits expanded pore size and layer spacing, lending to enhanced adsorption capabilities; (2) OTAB/Bt/TiO_2 displays an extended photoresponsive range, broadening its photocatalytic potential; (3) The presence of positively charged OTAB groups effectively counterbalances the negatively charged sites on the Bt surface. This positive charge on OTAB/Bt/TiO_2 facilitates the efficient adsorption of negatively charged SCN^- ions. Quenching experiments further demonstrated the pivotal role of abundant of h^+, •OH, and $•O^{2-}$ species catalytically generated by OTAB/Bt/TiO_2 under UV irradiation, contributing to the SCN^- degradation process. In addition, the OTAB/Bt/TiO_2 photocatalyst demonstrated good reusability as verified by four catalytic cycles. The efficient degradation of SCN^- and the complete mineralization of the intermediate product, CN^-, at the reaction's conclusion establish OTAB/Bt/TiO_2 as a secure and environmentally sustainable solution for the treatment of gold extraction tailing solutions.

Acknowledgements We acknowledge the financial supports by the National Natural Science Foundation of China (Grant No. 51874304); the Graduate Innovation Program of China University of Mining and Technology (2023WLKXJ164); "the Fundamental Research Funds for the Central Universities"(2023XSCX046); "the Postgraduate Research & Practice Innovation Program of Jiangsu Province" (KYCX23_2835).

Data Availability The datasets used and/or analyzed during the current study are available from the corresponding author upon reasonable request.

Declarations

Conflict of Interest The authors declare no competing interests.

References

Ajel, M. K., & Al-Nayili, A. (2022). Synthesis, characterization of Ag-WO3/bentonite nanocomposites and their application in photocatalytic degradation of humic acid in water. *Environmental Science and Pollution Research*. https://doi.org/10.1007/s11356-022-23614-4

Alkizwini, R. S., & Alquzweeni, S. S. (2021). Modeling natural bentonite, thermal-modified bentonite and iron-modified bentonite with artificial neural network, sorption kinetics and sorption isotherms for simulated sorption tetracycline. *International Journal of Environmental Science and Technology, 18*(9), 2633–2650. https://doi.org/10.1007/s13762-020-03004-4

Amaya, J., Suarez, N., Moreno, A., Moreno, S., & Molina, R. (2020). Mo or W catalysts promoted with Ni or Co supported on modified bentonite for decane hydroconversion. *New Journal of Chemistry, 44*(7), 2966–2979. https://doi.org/10.1039/c9nj04878b

Aminy, D. E., Rusdiarso, B., & Mudasir, M. (2022). Adsorption of Cd (II) ion from the solution using selective adsorbent of dithizone-modified commercial bentonite. *International Journal of Environmental Science and Technology, 19*(7), 6399–6410. https://doi.org/10.1007/s13762-021-03570-1

Anirudhan, T. S., & Ramachandran, M. (2015). Adsorptive removal of basic dyes from aqueous solutions by surfactant modified bentonite clay (organoclay): Kinetic and competitive adsorption isotherm. *Process Safety and Environmental Protection, 95*, 215–225. https://doi.org/10.1016/j.psep.2015.03.003

Azadi, S., Karimi-Jashni, A., Javadpour, S., & Amiri, H. (2020). Photocatalytic treatment of landfill leachate using cascade photoreactor with immobilized W-C-codoped TiO 2 nanoparticles. *Journal of Water Process Engineering*, *36*. https://doi.org/10.1016/j.jwpe.2020.101307

Bezsudnova, EYu., Sorokin, DYu., Tikhonova, T. V., & Popov, V. O. (2007). Thiocyanate hydrolase, the primary enzyme initiating thiocyanate degradation in the novel obligately chemolithoautotrophic halophilic sulfur-oxidizing bacterium Thiohalophilus thiocyanoxidans. *Biochimica et Biophysica Acta-Proteins and Proteomics, 1774*(12), 1563–1570. https://doi.org/10.1016/j.bbapap.2007.09.003

Bhattacharyya, K. G., & Sen Gupta, S. (2008). Adsorption of a few heavy metals on natural and modified kaolinite and montmorillonite: A review. *Advances in Colloid and*

Interface Science, 140(2), 114–131. https://doi.org/10.1016/j.cis.2007.12.008

Budaev, S. L., Batoeva, A. A., & Tsybikova, B. A. (2015). Degradation of thiocyanate in aqueous solution by persulfate activated ferric ion. *Minerals Engineering, 81*, 88–95. https://doi.org/10.1016/j.mineng.2015.07.010

Cao, X., Luo, S., Liu, C., & Chen, J. (2017). Synthesis of bentonite-supported Fe2O3-doped TiO2 superstructures for highly promoted photocatalytic activity and recyclability. *Advanced Powder Technology*. https://doi.org/10.1016/j.apt.2017.01.003

Chen, F., Yang, H., Luo, W., Wang, P., & Yu, H. (2017). Selective adsorption of thiocyanate anions on Ag-modified g-C3N4 for enhanced photocatalytic hydrogen evolution. *Chinese Journal of Catalysis, 38*(12), 1990–1998. https://doi.org/10.1016/S1872-2067(17)62971-1

Chen, W., Xiao, H., Xu, H., Ding, T., & Gu, Y. (2015). Photodegradation of methylene blue by TiO2-Fe3O4-bentonite magnetic nanocomposite. *International Journal of Photoenergy*. https://doi.org/10.1155/2015/591428

Combarros, R. G., Collado, S., Laca, A., & Diaz, M. (2015). Conditions and mechanisms in thiocyanate biodegradation. *Journal of Residuals Science & Technology, 12*(3), 113–124. https://doi.org/10.12783/issn.1544-8053/12/3/1

Du, Y., Niu, X., Bai, Y., Qi, H., Guo, Y., Chen, Y., et al. (2019). Synthesis of anatase TiO2 nanocrystals with defined morphologies from exfoliated nanoribbons: Photocatalytic performance and application in dye-sensitized solar cell. *ChemistrySelect, 4*(15), 4443–4457. https://doi.org/10.1002/slct.201900257

El-Korashy, S. A., Elwakeel, K. Z., & Abd El-Hafeiz, A. (2016). Fabrication of bentonite/thiourea-formaldehyde composite material for Pb(II), Mn(VII) and Cr(VI) sorption: A combined basic study and industrial application. *Journal of Cleaner Production, 137*, 40–50. https://doi.org/10.1016/j.jclepro.2016.07.073

García-García, F. A., Cristiani-Urbina, E., Morales-Barrera, L., Rodríguez-Peña, O. N., Hernández-Portilla, L. B., & Flores-Ortíz, C. M. (2023). Spectroscopic and microestructural evidence for T-2 toxin adsorption mechanism by natural bentonite modified with organic cations. *Toxins*. https://doi.org/10.3390/toxins15070470

Gao, K., Li, Y., & Na, P. (2020). Insight into design of MIL-125(Ti)-based composite with boosting photocatalytic activity: the embedded multiple Fe oxide count. *Advanced Materials Interfaces*, *7*(2). https://doi.org/10.1002/admi.201901449

Gao, Q., Yang, G., Jiang, Z., Ji, X., Yan, J., & Chen, J. (2019). Activated carbon adsorption combined with TiO_2 photocatalytic separation and purification of xylose from poplar wood pre-hydrolysate. *Transactions of China Pulp and Paper, 38*(11), 16–24.

Gu, J., Hu, X., Niu, Y., Xiu, S., Wang, J., & Li, Y. (2019). Experimental study of activated carbon/TiO_2 photocatalytic purification of indoor formaldehyde. *CIESC Journal, 48*(8), 1791–1794. https://doi.org/10.16581/j.cnki.issn1671-3206.2019.08.001

Guo, D., Feng, D., Zhang, Y., Zhang, Z., Wu, J., Zhao, Y., & Sun, S. (2022). Synergistic mechanism of biochar-nano TiO2 adsorption-photocatalytic oxidation of toluene. *Fuel Processing Technology*, *229*. https://doi.org/10.1016/j.fuproc.2022.107200

Haciyakupoglu, S., & Orucoglu, E. (2013). Se-75 radioisotope adsorption using Turkey's Resadiye modified bentonites. *Applied Clay Science, 86*, 190–198. https://doi.org/10.1016/j.clay.2013.10.010

He, H., Wu, T., Shu, X., Chai, K., Qiu, Z., Wang, S., & Yao, J. (2023). Enhanced organic contaminant retardation by CTMAB-modified bentonite backfill in cut-off walls: laboratory test and numerical investigation. *Materials*, *16*(3). https://doi.org/10.3390/ma16031255

Hirakawa, T., & Nosaka, Y. (2002). Properties of O-2(center dot-) and OH center dot formed in TiO2 aqueous suspensions by photocatalytic reaction and the influence of H2O2 and some ions. *Langmuir, 18*(8), 3247–3254. https://doi.org/10.1021/la015685a

Huang, J., Liu, Y., Jin, Q., Wang, X., & Yang, J. (2006). Adsorption studies of a water soluble dye, Reactive Red MF-3B, using sonication-surfactant-modified attapulgite clay. *Journal of Hazardous Materials*. https://doi.org/10.1016/j.jhazmat.2006.09.088

Huang, Z., Li, Y., Chen, W., Shi, J., Zhang, N., Wang, X., et al. (2017). Modified bentonite adsorption of organic pollutants of dye wastewater. *Materials Chemistry and Physics, 202*, 266–276. https://doi.org/10.1016/j.matchemphys.2017.09.028

Jiang, M., Zhang, M., Wang, L., Fei, Y., Wang, S., Nunez-Delgado, A., et al. (2022). Photocatalytic degradation of xanthate in flotation plant tailings by TiO2/graphene nanocomposites. *Chemical Engineering Journal*, *431*. https://doi.org/10.1016/j.cej.2021.134104

Kaleta, J., Papciak, D., & Puszkarewicz, A. (2013). Assessment of usability of bentonite clays for removing phenol from water solutions. *Rocznik Ochrona Srodowiska, 15*, 2352–2368.

Karavaiko, G., Kondrat'eva, T., Savari, E., Grigor'eva, N., & Avakyan, Z. (2000). Microbial degradation of cyanide and thiocyanate. *Microbiology, 69*(2), 167–173. https://doi.org/10.1007/BF02756193

Kaya, E. M. O., Ozcan, A. S., Gok, O., & Ozcan, A. (2013). Adsorption kinetics and isotherm parameters of naphthalene onto natural- and chemically modified bentonite from aqueous solutions. *Adsorption-Journal of the International Adsorption Society, 19*(2–4), 879–888. https://doi.org/10.1007/s10450-013-9542-3

Kuo, C.-Y., Jheng, H.-K., & Syu, S.-E. (2021). Effect of nonmetal doping on the photocatalytic activity of titanium dioxide on the photodegradation of aqueous bisphenol A. *Environmental Technology, 42*(10), 1603–1611. https://doi.org/10.1080/09593330.2019.1674930

Li, H. (2018). High sulfur cyanide wastewater treatment and common problems. *Tianjin Metallurgy, 6*, 49–52.

Jing-Yi, Li., Gao-Wa, S., & Li-Na, L. (2007). Photocatalytic degradation of organic pollutants on TiO2/bentonite. *Acta Physico-Chimica Sinica, 23*(1), 16–20. https://doi.org/10.3866/PKU.WHXB20070104

Li, X., Feng, X., Li, R., & Liu, W. (2022). Adsorption and photocatalytic properties of titanium dioxide/chitosan/bentonite composites for methylene blue. *Russian Journal of Inorganic Chemistry, 67*(SUPPL 2), S98–S113. https://doi.org/10.1134/S0036023622602124

Lin, M., Song, M., & Shen, X. (2012). Photocatalyst Tio(2) supported on bentonite for water organic pollutants

purification: a literature review. In W. Fan (Ed.), (Vol. 463–464, pp. 967-+). Presented at the Advanced Materials Research II, PTS 1 AND 2. https://doi.org/10.4028/www.scientific.net/AMR.463-464.967

Ma, L., Linghu, S., Chen, Z., Wang, S., Gu, H., Pan, T., & Chen, X. (2023). Coupled use of modified bentonite and urea hydrogen peroxide to degrade paraxylene. *Water Air and Soil Pollution*, *234*(4). https://doi.org/10.1007/s11270-023-06225-8

Maxim, L. D., Niebo, R., & McConnell, E. E. (2016). Bentonite toxicology and epidemiology - a review. *Inhalation Toxicology, 28*(13), 591–617. https://doi.org/10.1080/08958378.2016.1240727

Dlamini, M. C., Dlamini, M. L., Mente, P., Tlhaole, B., Erasmus, R., Maubane-Nkadimeng, M. S., & Moma, J. A. (2022). Photocatalytic abatement of phenol on amorphous TiO2-BiOBr-bentonite heterostructures under visible light irradiation. *Journal of Industrial and Engineering Chemistry*. https://doi.org/10.1016/j.jiec.2022.04.023

Mishra, A., Sharma, M., Mehta, A., & Basu, S. (2017). Microwave treated bentonite clay based TiO2 composites: An efficient photocatalyst for rapid degradation of methylene blue. *Journal of Nanoscience and Nanotechnology, 17*(2), 1149–1155. https://doi.org/10.1166/jnn.2017.12674

Olafadehan, O. A., Bello, V. E., & Amoo, K. O. (2022). Production and characterization of composite nanoparticles derived from chitosan, CTAB and bentonite clay. *Chemical Papers, 76*(8), 5063–5086. https://doi.org/10.1007/s11696-022-02228-7

Pan, X., Li, Y., Huang, H., Ren, Y., & Wang, C. (2009). Biodegradation of thiocyanide in coking wastewater and its interaction with phenol and ammonia nitrogen. *CIESC Journal, 60*(12), 3089–3096.

Pandey, S. (2017). A comprehensive review on recent developments in bentonite-based materials used as adsorbents for wastewater treatment. *Journal of Molecular Liquids, 241*, 1091–1113. https://doi.org/10.1016/j.molliq.2017.06.115

Saleh, S., Mohammadnejad, S., Khorgooei, H., & Otadi, M. (2021). Photooxidation/adsorption of arsenic (III) in aqueous solution over bentonite/chitosan/TiO2 heterostructured catalyst. *Chemosphere*, *280*. https://doi.org/10.1016/j.chemosphere.2021.130583

Selim, K., Rostom, M., Youssef, M., Abdel-Khalek, N., Abdel-Khalek, M., & Hassan, E. (2020). Surface modified bentonite mineral as a sorbent for Pb2+ and Zn2+ ions removal from aqueous solutions. *Physicochemical Problems of Mineral Processing, 56*(6), 145–157. https://doi.org/10.37190/ppmp/127833

Soegijono, C. J. B. (2017). Investigation of intercalation of sodium-montmorillonite with octadecyl trimethyl ammonium bromide surfactant. *Jurnal Vokasi Indonesia*. https://doi.org/10.7454/jvi.v5i1.106

Tai, M., Tang, H., Li, W., Feng, G., Zhang, S., Wang, N., & Pei, J. (2007). Advances in the treatment of cyanide in gold mine wastewater and tailings. *China Resources Comprehensive Utilization, 2*, 22–25.

Tomic, Z., Asanin, D., Durovic-Pejcev, R., Dordevic, A., & Makreski, P. (2015). Adsorption of acetochlor herbicide on inorganic- and organic-modified bentonite monitored by mid-infrared spectroscopy and batch adsorption. *Spectroscopy Letters, 48*(9), 685–690. https://doi.org/10.1080/00387010.2014.962705

Vohra, M. S. (2011). removal of thiocyanate from synthetic wastewater using TiO2 mediated photocatalytic degradation process. *Fresenius Environmental Bulletin, 20*(5A), 1308–1313.

Wang, C., Shi, H., & Li, Y. (2012). Preparation of bentonite supported nano titanium dioxide photocatalysts by electrostatic self-assembly method. *Journal of Wuhan University of Technology-Materials Science Edition, 27*(4), 603–607. https://doi.org/10.1007/s11595-012-0513-4

Wu, T., Sun, D., Li, Y., Zhang, H., & Lu, F. (2011). Thiocyanate removal from aqueous solution by a synthetic hydrotalcite sol. *Journal of Colloid and Interface Science, 355*(1), 198–203. https://doi.org/10.1016/j.jcis.2010.11.058

Yuan, J., Chang, Y., Zheng, C., Yang, X., Wang, W., & Xie, F. (2021). A review of cyanide tailings decyanidation technology. *The Chinese Journal of Nonferrous Metals, 31*(6), 1568–1581.

Zhuang, X., Li, X., Yang, Y., Wang, N., Shang, Y., Zhou, Z., et al. (2020). Enhanced sulfamerazine removal via adsorption-photocatalysis using Bi2O3-TiO2/PAC ternary nanoparticles. *WATER*, *12*(8). https://doi.org/10.3390/w12082273